ARTICLE

Optoelectronic Properties of Nanostructured Ensembles Controlled by Biomolecular Logic Systems

Marcos Pita,[†] Melina Krämer,[†,‡] Jian Zhou,[†] Arshak Poghossian,[‡] Michael J. Schöning,[‡] Víctor M. Fernández,[§] and Evgeny Katz[†,*]

[†]Department of Chemistry and Biomolecular Science, and NanoBio Laboratory (NABLAB), Clarkson University, Potsdam, New York 13699-5810, [‡]Institute of Nano- and Biotechnologies (INB), Aachen University of Applied Sciences, Ginsterweg 1, D-52428 Jülich, Germany, and Institute of Bio- and Nanosystems (IBN2), Research Centre Jülich, D-52425 Jülich, Germany, and [§]Instituto de Catálisis y Petroleoquímica, CSIC, C/Marie Curie 2, 28049 Cantoblanco, Madrid, Spain

ABSTRACT A nanostructured system composed of enzyme-functionalized silica microparticles, *ca.* 74 μm, and gold-coated magnetic nanoparticles, 18 ± 3 nm, modified with pH-sensitive organic shells was used to process biochemical signals and transduce the output signal into the changes of the optoelectronic properties of the assembly. The enzymes (glucose oxidase, invertase, esterase) covalently bound to the silica microparticles performed Boolean logic operations AND/OR processing biochemical information received in the form of chemical input signals resulting in changes of the solution pH value. Dissociation state of the organic shells on the gold-coated magnetic nanoparticles was controlled by pH changes generated *in situ* by the enzyme logic systems. The charge variation on the organic shells upon the reversible protonation/dissociation process resulted in the changes of the gold layer localized surface plasmon resonance energy (LSPR), thus producing optical changes in the system. The proton transfer process allowed the functional coupling of the information processing enzyme systems with the signal transducing gold-coated magnetic nanoparticles providing their cooperative performance. Magnetic properties of the gold-coated magnetic nanoparticles allowed separation of the signal-transducing nanoparticles from the enzyme-modified signal processing silica microparticles. The reversible system operation was achieved by the Reset function, returning the pH value and optical properties of the system to the initial state. This process was biocatalyzed by another immobilized enzyme (urease) activated with a biochemical signal. The studied approach opens the way to novel optical biosensors logically processing multiple biochemical signals and "smart" multisignal responsive materials with logically switchable optical properties.

KEYWORDS: functional nanoparticles · magnetic nanoparticles · enzyme logic · logic gate · signal-responsive material · localized surface plasmon resonance · LSPR · switchable optical properties · optoelectronic properties · nanostructured materials

Experimental and theoretical studies of optoelectronic properties of nanostructured materials[1] and, particularly, ensembles of metallic nanoparticles (NPs) in solutions and on surfaces[2] have attracted much recent attention. Localized surface plasmon resonance (LSPR) in metal NPs, which controls their optical properties, depends on the metal nature, shape, size, and environment of the NPs.[3] Minor changes in the distances between the NPs, charges localized on them, or alteration of charging/dielectric properties in their nearby environment (particularly changes of charges in the organic shells)[4] might be substantially amplified by the variation of the optoelectronic properties of NPs (*i.e.*, LSPR) yielding a shift of their absorbance band. Functional coupling of metal NPs with biomolecular systems[5] and high sensitivity of the optoelectronic properties of metal NPs to the environment changes are used in various sensors and biosensors,[6,7] specifically in DNA and protein sensors,[8] and enzyme-based biosensors.[9] Most of the observed optical effects and the applications based on them originate from the distance variation between metal NPs resulting in the change of their plasmon coupling and consequently in the absorbance shift in the NPs spectra.[10] The distance variation could be caused by cross-linking of the biomolecular-functionalized NPs through biospecific interactions (usually upon DNA hybridization[11] or protein-affinity binding[12]). Charging effects on the LSPR energy and therefore on the optical properties of metal NPs are much less studied and rarely used in biosensors and optobioelectronic systems. The charge directly associated with the metallic cores of NPs or distributed on a short distance from them (*e.g.*, associated with the organic shell) could be changed by chemical,[13] biochemical,[14] electrochemical,[15,16] or photochemical[17] means. However, the charge effect on the NPs absorbance band shift was reported only in a few papers,[15] while other studies used surface plasmon resonance to observe the charge effects on the optical properties of surface-confined NPs.[14,17] Functional coupling of metal NPs with biomolecular systems through the charge transfer processes resulting in the optical properties variation is a challenging aim yet.

*Address correspondence to ekatz@clarkson.edu.

Received for review July 20, 2008 and accepted September 19, 2008.

Published online October 1, 2008. 10.1021/nn8004558 CCC: $40.75

Enzyme-based biocomputing systems mimicking Boolean logic operations were pioneered recently.[18,19] They accept biochemical input signals, logically process them, and generate an output signal in the form of chemical changes dependent on the combination of all applied chemical input signals and on the built-in biochemical "program". The compatibility of the biochemical logic gates allows them to assemble in the form of complex biocomputing networks composed of several concatenated logic units processing large amount of various combinations of biochemical signals.[20,21] The possibility to scale up logic systems is the most important advantage of the enzyme-based ensembles[22] over other chemical computing systems.[23,24] The enzyme-based logic gates were already coupled with electronic transducers (modified electrodes) by means of electron transfer processes.[25] The present paper describes a new approach to the coupling between the enzyme logic systems and a signal-responsive nanostructured material through proton transfer processes.

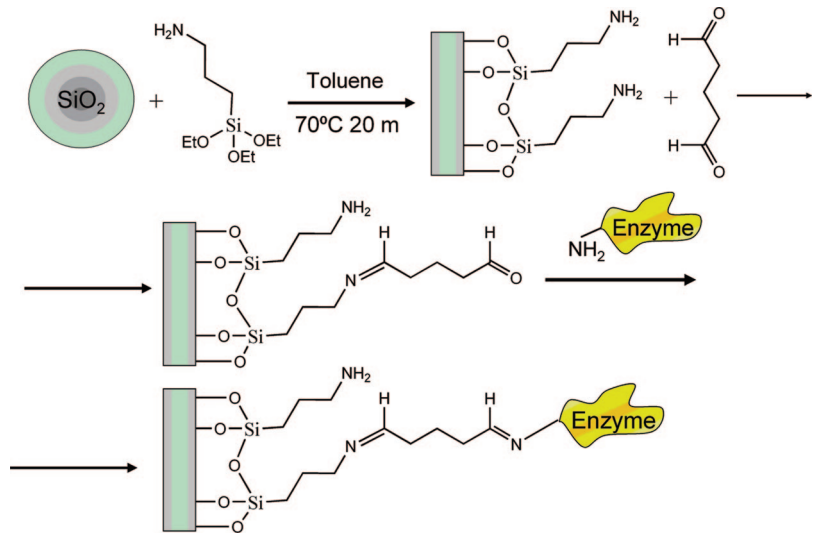

Scheme 1. Modification of the silica microparticles with the enzymes.

RESULTS AND DISCUSSION

The studied hybrid systems were composed of two kinds of modified particles functionally coupled together: the enzyme-functionalized silica microparticles (*ca.* 74 μm) logically processing biochemical signals, and the Au-coated magnetic NPs (18 ± 3 nm) transducing the enzyme-generated *in situ* pH changes to the alteration of their optoelectronic properties upon charging/discharging pH-sensitive organic shells. The superparamagnetic properties of the signal-transducing NPs were used to keep them suspended in a solution upon application of an external magnetic field (a NdFeB magnet was placed 1 cm above the NP suspension to generate a magnetic field of *ca.* 2 kG on the solution surface), thus preventing their precipitation, which could result in the uncontrolled changes of their optical properties. The enzymes performing logic operations were immobilized on the silica microparticles to prevent the enzyme adsorption on the signal-transducing Au-coated magnetic NPs, which might result in their uncontrolled aggregation. The enzyme-functionalized silica microparticles were sedimented at the bottom of the reacting vial and thus separated from the signal-transducing magnetic NPs suspended in the solution. The bicomponent hybrid system provided stable and reproducible optical properties controlled by pH values of the solution produced *in situ* upon the enzyme logic operations.

Four kinds of the enzyme-functionalized silica NPs were prepared to assemble the enzyme logic gates and to reset the system. The surface of the silica microparticles was silanized with γ-aminopropyl-triethoxysilane (APTES) to introduce amino functional groups, and then glutaric dialdehyde coupling was used to immobilize covalently (*via* formation of Schiff base links) four different enzymes on the microparticles: glucose oxidase (GOx), invertase (Inv), esterase (Est), and urease (Ur) (Scheme 1). The first three immobilized enzymes were used to assemble logic gates, and urease was applied to reset the system to the initial conditions. The enzyme information processing systems were then assembled as mixtures of various enzyme-modified silica microparticles taken in specific ratios. Two enzyme logic systems processing biochemical signals were assembled in this study: (*i*) The **AND**/**Reset** logic gate was composed of three enzymes covalently bound to

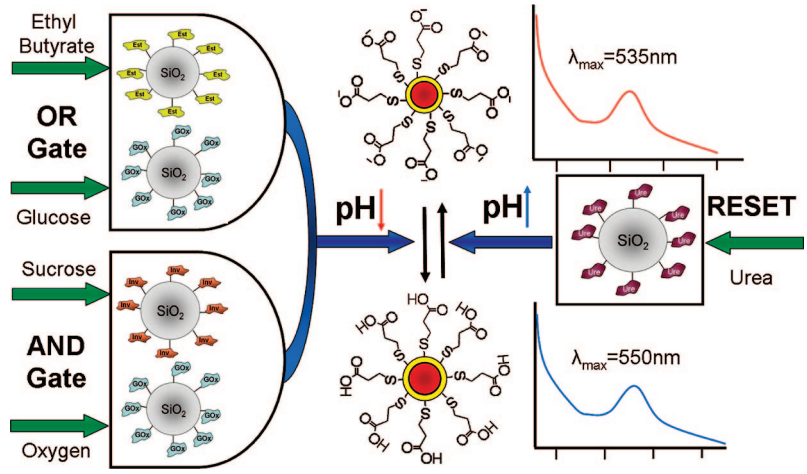

Scheme 2. Hybrid systems composed of the enzyme logic units covalently bound to the silica microparticles and the pH-sensitive Au-coated/magnetic core NPs transducing the pH changes generated by the enzymes into the optical changes.

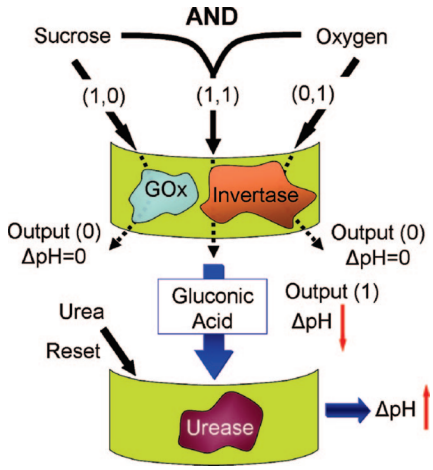

Scheme 3. Operation of the AND−Reset enzyme logic system.

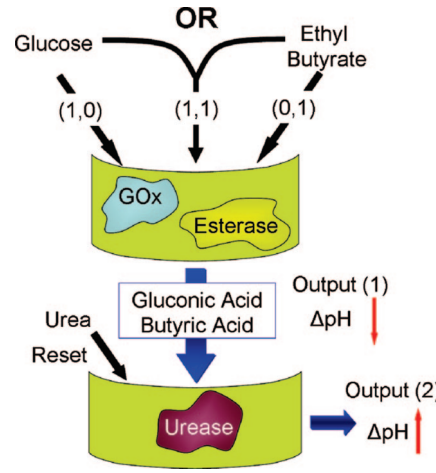

Scheme 4. Operation of the OR−Reset enzyme logic system.

the silica NPs: Inv (1.2 units), GOx (0.8 units), and Ur (2.3 units). (*ii*) The **OR**/**Reset** logic gate was also composed of three enzymes immobilized on the silica microparticles: GOx (0.8 units), Est (0.2 units), and Ur (2.3 units), Scheme 2. The **AND** gate was activated by two chemical input signals: sucrose (100 mM) and oxygen (concentration obtained in the solution under equilibrium with air) (Scheme 3). The input signals were considered to be "**0**" in the absence of the respective chemicals (Ar was bubbled through the solution in order to remove O_2 when needed), while the input signals were "**1**" in the presence of the added chemicals at the selected concentrations. The operating concentrations of the chemical inputs were selected to produce substantial pH changes in a nonbuffered solution (1 mM NaCl) upon the biochemical reactions. Similarly to the digitalization of electronic signals used in electronics, we considered the intermediate values of the concentrations of the chemical inputs as undefined signals. Global mapping of the logic gate transduction function upon application of variable concentrations of the chemical input signals[22] was outside the scope of the present study. If the variable input concentrations were applied, this would allow the optimization of the gate performance function.[22] The biochemical chain reaction proceeding in the **AND** logic gate in the presence of sucrose and O_2 (input signals: "**1**,**1**") included the hydrolytic conversion of sucrose to glucose and fructose biocatalyzed by Inv, followed by glucose oxidation biocatalyzed by GOx to yield gluconic acid. The final product, gluconic acid, produced by the chain reaction resulted in the acidification of the solution-lowering pH from the initial value of pH 7.0 to the final pH value of *ca.* pH 4. Obviously, the biochemical chain reaction was not completed in the absence of sucrose or O_2 or both of them (input signals: "**0**,**1**", "**1**,**0**", "**0**,**0**", respectively), thus inhibiting the formation of gluconic acid and keeping the pH value unchanged. The output signal generated by the system in the form of the pH changes was considered as "**1**" if $\Delta pH > 2$, while $\Delta pH < 0.2$ was considered as "**0**" output signal. The pH changes between 0.2 and 2 thresholds were considered as undefined (similarly to the approach used in electronics). To complete the reversible cycle, the **Reset** operation was activated by the addition of urea (2 mM), resulting in the formation of ammonia biocatalyzed by urease. This resulted in the increase of the pH reaching the pH value of *ca.* 6.5−7.0.

The **OR** gate operation was activated by two chemical input signals: glucose (10 mM) or/and ethyl butyrate (10 mM), considered to be "**1**" at the selected concentrations and "**0**" in the absence of the chemicals (Scheme 4). The **OR** enzyme logic gate performed two parallel reactions: glucose oxidation biocatalyzed by GOx to yield gluconic acid (O_2 serving as a natural electron acceptor was always in the system) and hydrolysis of ethyl butyrate biocatalyzed by Est producing butyric acid. Any or both of the reactions (input signals: "**0**,**1**", "**1**,**0**", "**1**,**1**") resulted in the formation of acids, thus lowering the pH value from the initial value of pH 7.0 to the final value of *ca.* pH 4. Obviously, in the absence of both chemical inputs (input signals: "**0**,**0**"), both reactions were inhibited, thus leaving the initial pH value unchanged. The **Reset** operation that returned pH to the initial value was activated by the addition of urea similarly to the described above.

The pH changes produced upon logical processing of the chemical input signals were transduced into optical signals by the functional Au-coated magnetic NPs added to the system (0.1 mg · mL; Scheme 2). The NPs (18 ± 3 nm diameter) were composed of cobalt ferrite ($CoFe_2O_4$) superparamagnetic core (13 ± 2 nm, saturated magnetization ~70 emu · g^{-1}) coated with a gold shell modified with a mercaptopropionic acid monolayer. Three parts of the NPs were used for different functions: (*i*) The organic shell composed of mercaptopropionic acid chemisorbed on the Au layer was responsible for changing the charge upon the pH changes. This originated from the dissociation equilib-

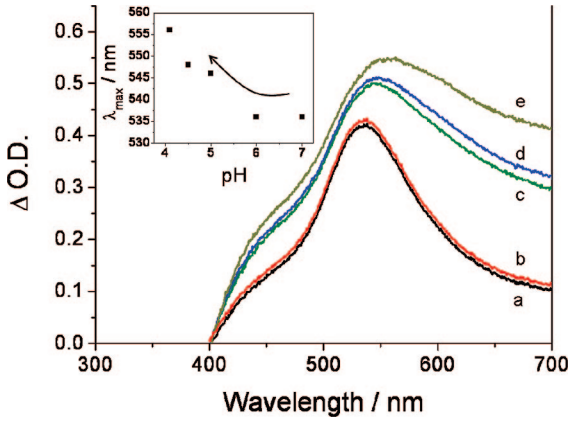

Figure 1. Spectra of the Au-coated/magnetic core NPs suspension (450 mg, 4 mL) recorded in the presence of the enzyme AND logic system upon the "1,1" input signals resulting in the decreasing pH values: (a) 7.0, (b) 6.0, (c) 4.9, (d) 4.4, (e) 4.0. Inset: shift of the λ_{max} upon the pH changes generated *in situ* by the enzyme logic system.

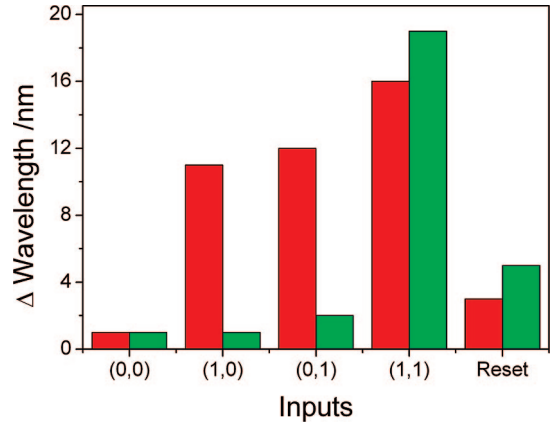

Figure 2. Optical output signals ($\Delta\lambda_{max}$) generated in the system upon various combinations of the chemical input signals: the enzyme OR logic gate (red) the enzyme AND logic gate (green).

rium of the carboxylic groups associated with the shell monolayer. (*ii*) The Au thin film generated the optical signals upon variation of the localized surface plasmon (LSPR) energy controlled by the charge on the organic shell. (*iii*) The magnetic cores were needed to keep the NPs suspended in the solution upon application of an external magnetic field, thus preventing their precipitation and aggregation with the enzymatic systems.

The absorbance spectra of the Au-coated magnetic NPs were recorded at different pH values produced in the solution upon *in situ* performed biocatalytic reactions induced by various chemical input signals logically processed by the enzyme systems. The pK_a value of mercaptopropionic acid in a monolayer configuration is known to be *ca.* 5.2 ± 0.1.[26] The experiments were always started at pH 7.0 where the carboxylic groups of the shell are dissociated (negatively charged). Upon applying chemical input signals processed by the enzyme logic gates, the initial pH value was decreased, reaching the pH value of *ca.* 4 (if the biocatalytic reactions were activated), or remained unchanged (if the reactions did not proceed) depending on the combination of the chemical input signals. The acidic pH generated *in situ* resulted in the protonation of the shell carboxylic groups converting them to the neutral state. The change of the electric charge associated with the shell induced change of the LSPR energy reflected by the shift of the absorbance peak in the optical spectrum of the system. Figure 1 shows the typical spectra changes observed upon the biocatalytic reactions induced in the **AND** logic gate when the combination of the chemical input signals "**1**,**1**" was applied. The absorbance maximum was shifted to longer wavelengths reaching the Δλ of 21 nm (Figure 1, inset). Obviously, the combinations of the input signals "**0**,**0**", "**0**,**1**", and "**1**,**0**" processed by the **AND** gate did not result in detectable alterations of the spectrum (Δλ < 2 nm). After reaching the final shift of the pH and respective optical change, the **Reset** function was applied, returning the absorbance to almost original wavelength. The optical responses produced by the system upon application of different combinations of the input signals corresponded to the logical behavior of **AND**−**Reset** function (Figure 2). Figure 3 shows the typical spectra changes upon the biocatalytic reactions induced in the **OR** logic gate when the combinations of the chemical input signals "**0**,**1**", "**1**,**0**", or "**1**,**1**" were applied (no optical changes were observed in the case of "**0**,**0**" inputs). The absorbance maximum was shifted to longer wavelengths reaching Δλ of 15 nm (Figure 3, inset). After reaching the final shift of the pH and respective optical change, the **Reset** function was applied, returning the absorbance to almost original wavelength. The optical responses produced by the system upon application of different combinations of the input signals corresponded to the logical behavior of **OR**−**Reset** function (Figure 2).

The mechanism responsible for the transduction of the pH variation into the optical changes needs seri-

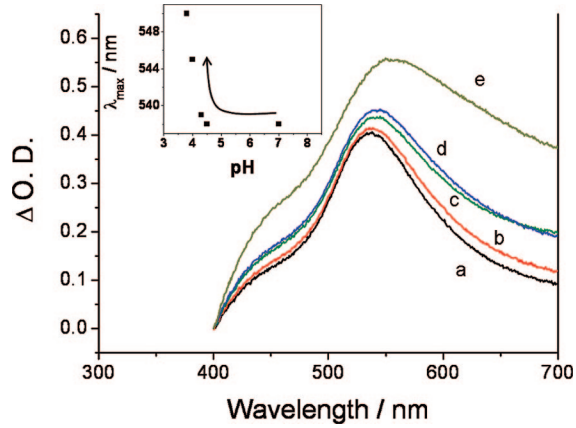

Figure 3. Spectra of the Au-coated/magnetic core NPs suspension (450 mg, 4 mL) recorded in the presence of the enzyme OR logic system upon the "0,1", "1,0", "1,1" input signals resulting in the decreasing pH values: (a) 7.0, (b) 4.5, (c) 4.15, (d) 4.0, (e) 3.8. Inset: The shift of the λ_{max} upon the pH changes generated *in situ* by the enzyme logic system.

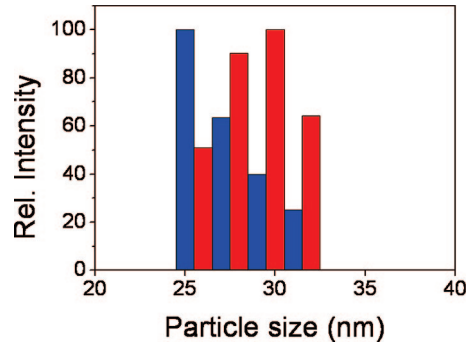

Figure 4. Effective sizes of the Au shell/magnetic core NPs measured by the dynamic light scattering (DLS) at different pH values generated *in situ* by the enzyme logic systems: pH 4.0 (red) and pH 7.0 (blue).

ous discussion. An obvious and trivial explanation of the observed optical changes could be the reversible aggregation/dissociation of the NPs upon discharging/charging their shells because of the protonation/dissociation of the carboxylic groups at different pH values. Indeed, lowering pH results in the protonation of the carboxylic groups yielding neutral NPs capable of aggregating. The aggregation process would induce the "red" shift in the spectra[11,12] similar to that observed in our experiments. Increasing pH would result in the dissociation of the carboxylic groups inducing their negative charging and dissociation, thus returning the initial optical properties. To verify this option, we performed dynamic light scattering (DLS) measurements for the NP suspension at pH 7.0 and 4.0, where the spectra have the biggest difference. It has been found that the NPs have almost the same size distribution between 24 and 32 nm (Figure 4), thus disapproving the aggregation/dissociation mechanism for the optical changes. It should be noted that the effective size of the NPs was bigger than their sizes observed by TEM[27,28] due to the fact that DLS detects the hydrodynamic radii instead of the particle size itself.

A much more intriguing mechanism would be the dependence of the LSPR energy and thus optical features of the Au layer on the charge associated with the organic shell. In this case, the shift in the plasmon frequency and the respective shift of the λ_{max} in the absorbance spectrum are promoted by the change of the charge upon protonation−deprotonation of the mercaptopropionic acid monolayer attached to the NPs surface. This charge alters the electron density in the NPs surface (Thomson−Fermi layer). Consequently, the dielectric constant is altered proportionally to the electron density. To estimate the effect of the negatively charged surface when the shell monolayer is deprotonated, rough calculations were performed. Upon irradiation of the Au-coated magnetic NPs with an electromagnetic wave, the free electrons are driven by the electric field to coherently oscillate at the plasma frequency, ω_p. The typical expression for ω_p in bulk metal can be formulated as following (eq 1):[29]

$$\omega_p = \left(\frac{N \cdot e^2}{\varepsilon_0 m_e}\right)^{1/2} \quad (1)$$

where N is the density of electrons, ϵ_0 is the dielectric constant of vacuum, and e and m_e are the charge and mass of an electron, respectively. The initial electron density, $N_{535} = 3.13 \times 10^{-7}\ e^- \cdot m^{-3}$, was derived using eq 1 for $\lambda_{max} = 535$ nm at pH 7.0 when the shell around the NPs exists in the dissociated (negatively charged) state, while $N_{550} = 2.96 \times 10^{-7}\ e^- \cdot m^{-3}$ was derived for $\lambda_{max} = 550$ nm at pH 4.0 when the shell is protonated (neutral). Therefore, the increase of the electron density upon protonation of the carboxylic groups in the shell was $\Delta N = 1.7 \times 10^{-8}\ e^- \cdot m^{-3}$. The NPs show an average composition of a 15 nm diameter $CoFe_2O_4$ core and a 3 nm thick Au shell. As the density of $CoFe_2O_4$ is 5.3 $g \cdot cm^{-3}$ and gold's density is 19.3 $g \cdot cm^{-3}$, the average density of the NPs can be calculated as follows (eq 2):

$$\rho_{particle} = \rho_{CoFe_2O_4} \cdot \chi_{CoFe_2O_4} + \rho_{Au} \cdot \chi_{Au} \quad (2)$$

where ρ_i corresponds to the density of the specific materials and χ_i to the fraction of volume occupied by the material in the NPs. The result gives the density, $\rho_{particle} = 17.71\ g \cdot cm^{-3}$, of the composite NPs. The volume of a single NP (diameter 18 nm) is ca. 3×10^3 nm^3. Thus, taking into account the NPs concentration (0.5 $mg \cdot mL^{-1}$, $\sim 10^{13}$ $NPs \cdot mL^{-1}$), one can estimate the number of NPs in the reacting solution (4 mL), $\sim 4 \times 10^{13}$ NPs, and their total volume, $\sim 1.2 \times 10^{-10}$ m^3. The number of electrons depleted upon the LSPR change, *ca.* 140 electrons per NP, was derived by dividing ΔN by the total volume of the NPs. On the other side, the density of mercaptopropionic acid in the shell monolayer could be roughly estimated as 7.6×10^{-10} $mol \cdot cm^{-2}$ or 1.26×10^{13} $molecules \cdot cm^{-2}$.[30] Taking into account the surface area of a single NP, 4000 nm^2, the number of the carboxylic groups in the shell of a single NP is *ca.* 126. This rough calculation shows a good agreement between the charge variation responsible for the LSPR shift (*ca.* 140 electrons per NP) and the number of dissociating groups in the shell (*ca.* 126), thus giving confirmation that the charging/discharging process in the shell is responsible for the optical changes in the system.

CONCLUSIONS

The enzyme logic systems were used to process biochemical information received in the form of chemical input signals resulting in pH changes produced *in situ* upon biocatalytic reactions. The Au shell/magnetic core NPs functionalized with the dis-

sociating organic monolayer were used to transduce the pH changes into the variation of their optoelectronic properties. The LSPR shift recorded in the optical spectra of the NPs was used to read out the results of the enzyme logic operations. Two logic operations (**AND**/**OR**) followed by the **Reset** function were performed in the present study. The flexibility of enzyme logics allowing various logic operations[19] and the possibility to scale up[22] the enzyme logic systems in the form of complex logic networks[21] promises almost unlimited variability and complexity of the biochemical information−processing systems. Coupling of the biochemical logics with signal-transducing elements changing the bulk material properties in response to the enzyme logic operations opens the way to novel signal-processing systems. Application of the nanostructured signal-responsive systems is of particular interest due to the possibility to scale down the responsive elements to a single nanounit (*e.g.*, a single-responsive nanoparticle). Variation of the optoelectronic properties of nanoparticles and quantum dots in response to the enzyme logic operations is a promising direction in the general avenue of the biochemical logics. Besides the fundamental scientific interest, potential applications in optobioelectronics, biosensors, and medical imaging are envisaged.

EXPERIMENTAL SECTION

Chemicals: All chemicals and enzymes were purchased and used without further purification. The enzyme logic gates were built with the following enzymes purchased from Sigma-Aldrich: glucose oxidase (GOx) from *Aspergillus niger*, type X-S (E.C. 1.1.3.4); esterase (Est) from porcine liver (E.C. 3.1.1.1), crude; invertase (Inv) from bakers yeast, grade VII (E.C. 3.2.1.26); and urease from jack beans (E.C. 3.5.1.5). Other chemicals purchased from Sigma-Aldrich (ACS quality) were γ-aminopropyl-triethoxysilane (APTES), γ-mercaptopropyl-trimethoxysilane (MPTMS), $HAuCl_4$, β-D-(+)-glucose, urea, glutaric dialdehyde aqueous solution (50% w/v), and sucrose. Ethyl butyrate and 3-mercaptopropionic acid (MPA) were purchased from Fluka. Ferric chloride ($FeCl_3 \cdot 6H_2O$), ferric nitrate ($Fe(NO_3)_3 \cdot 9H_2O$), hydroxylamine hydrochloride ($NH_2OH \cdot HCl$), hydrochloric acid, sodium hydroxide, and disodium phosphate monobasic were purchased from Fisher Scientific. Cobalt chloride hexahydrate ($CoCl_2 \cdot 6H_2O$), sodium phosphate dibasic monohydrate, sodium chloride crystal, and toluene were purchased from J.T. Baiker. Ethanol was from Pharmco-AAPER. Silica nanoparticles (200 mesh, *ca.* 74 μm diameter) were purchased from MO-SCI Specialty Products, LLC. All aqueous solutions were prepared with ultrapure water (18.2 MΩ) from NANOpure Diamond (Barnstead) source.

Au-Coated Magnetic NP Synthesis: Gold-coated magnetic NPs were synthesized according to the recently developed procedure[27,28] (see details in the Supporting Information): Briefly, cobalt ferrite ($CoFe_2O_4$) NPs were prepared by coprecipitation of $CoCl_2$ and $FeCl_3$ salts under alkaline environment.[31,32] The cobalt ferrite ferrofluid was functionalized with amino and thiol groups by condensation of silane coupling reagents APTES and MPTMS. The resulting functionalized NPs were incubated at pH 4 in the presence of Au NPs (diameter 3 nm) synthesized according to the published procedure.[33] The Au NPs covalently attached to the magnetic cores through thiol groups acted as nucleation seeds for further iterative reduction of gold(III) ions with hydroxylamine[34] to yield the Au shell/magnetic core NPs. The size of the Au-coated magnetic NPs, 18 ± 3 nm, was measured by TEM imaging.[35]

Organic Shell Formation: Au-coated magnetic NP dispersion in water (4 mL; 0.5 mg · mL^{-1}) was reacted with MPA, 1 mM, for 3 h at room temperature. The modified NPs were washed with three cycles of centrifugation (6000 rpm, 20 min) at room temperature. After decantation of the supernatant and re-dispersion in an aqueous NaCl, 1 mM, solution, they were treated with ultrasound for 2 min to yield the stable dispersion.

Enzyme Immobilization on Silica NPs: Enzymes were covalently immobilized on the silica microparticles through a three-step immobilization process. First, 150 mg of silica particles was reacted with a 5 mL of toluene solution containing 1% v/v APTES under a gentle shaking for 20 min at 70 °C. Then the dispersion was centrifuged (1500 rpm, 1 min, room temperature); the supernatant was separated, and the particles were re-dispersed. This process was performed three times in toluene, twice in ethanol, and three times in 1 mM phosphate buffer, pH 7, to purify the silanized silica microparticles. The amino-functionalized silica particles (1 g) were reacted with an aqueous solution of glutaric dialdehyde (4 mL, 10% w/v) for 30 min upon shaking, then they were washed five times with 0.1 M phosphate buffer, pH 7, by centrifugation (1500 rpm, 1 min, room temperature). The enzymes were immobilized on the aldehyde-functionalized silica microparticles by reaction of 20 units of each enzyme with 150 mg of microparticles for 30 min under gentle shaking at room temperature. The enzyme-functionalized particles were washed five times with NaCl solution, 1 mM, by using the centrifuge (1500 rpm, 1 min, room temperature). The biocatalytic activities of the enzymes immobilized on the silica microparticles were found following the rates of pH changes produced upon the biocatalytic reactions: GOx, 5.3 units · μg^{-1}, Inv, 8.0 units · μg^{-1}, Est, 1.3 units · μg^{-1}, and Ur, 15.3 units · μg^{-1} (see details in the Supporting Information). The experimental values of the enzymatic activity correlate with the theoretically estimated activities expected for monolayer coverage of the enzymes on silica microparticles, assuming that the enzyme natural activities were barely affected by the immobilization process.

Enzyme Logic Gate Composition and Operation: Two different enzyme logic gates were designed for the pH control. The biochemical "machinery" of the logic gates was defined as an aqueous solution (NaCl, 4 mL, 1 mM) containing 450 mg of silica microparticles modified with the enzymes (150 mg per specific enzyme): GOx (0.8 units), Inv (1.2 units), and Ur (2.3 units) for the **AND**−**Reset** system, and GOx (0.8 units), Est (0.2 units), and Ur (2.3 units) for the **OR**−**Reset** system. The input signals were defined as sucrose (100 mM; input **A**) and O_2 (the concentration in the equilibrium with air; input **B**) for the **AND** gate; glucose (10 mM; input **A**) and ethyl butyrate (10 mM; input **B**) for the **OR** gate; urea (2 mM) for the **Reset** function. The enzyme-modified microparticles were sedimented at the bottom of the vial under a gentle magnetic stirring to enhance the diffusional enzymatic reactions. Au-coated magnetic NPs modified with MPA monolayer organic shells were dispersed in the same solution at the concentration of 0.1 mg · mL. To avoid the contact and further adsorption of the NPs on the enzyme-modified silica microparticles, a NdFeB magnet was placed 1 cm above the solution, producing the magnetic field of *ca.* 2 kG at the top of the solution, keeping the magnetic NPs suspended. The initial pH value of the system was adjusted to pH 7.0 with HCl, 1 mM, prior to the addition of the chemical input signals. Then different combinations of the chemical input signals were added to the system, and the pH values and spectra were recorded at different time intervals of the proceeding reactions. Before the absorbance spectrum was recorded, the sample was immersed in an ultrasound bath for 1 min. Once the limit of pH acidification was reached, the **Reset** function was activated by the injection of the urea.

Instrumentation: The absorbance spectra were recorded using a Shimadzu UV-2450PC spectrophotometer. The pH evolutions were monitored with a Mettler Toledo SevenEasy pH meter. DLS

measurements were conducted using "90 Plus Particle Size Analyzer" from Brookhaven Instruments Corporation. All measurements were performed at 23 ± 2 °C.

Acknowledgment. This research was supported by the NSF grants "Signal-Responsive Hybrid Biomaterials with Built-in Boolean Logic" (DMR-0706209) and "Biochemical Computing: Experimental and Theoretical Development of Error Correction and Digitalization Concepts" (CCF-0 726698).

Supporting Information Available: Experimental details for the NPs modification and analysis of the biocatalytic activity of the immobilized enzymes. This material is available free of charge *via* the Internet at http://pubs.acs.org.

REFERENCES AND NOTES

1. Murray, W. A.; Barnes, W. L. Plasmonic Materials. *Adv. Mater.* **2007**, *19*, 3771–3782.
2. Shipway, A. N.; Katz, E.; Willner, I. Nanoparticle Arrays on Surfaces for Electronic, Optical, and Sensor Applications. *ChemPhysChem* **2000**, *1*, 18–52.
3. Moores, A.; Goettmann, F. The Plasmon Band in Noble Metal Nanoparticles: An Introduction to Theory and Applications. *New J. Chem.* **2006**, *30*, 1121–1132.
4. Maier, S. A. *Plasmonics: Fundamentals and Applications*; Springer: New York, 2007.
5. Katz, E.; Willner, I. Integrated Nanoparticle-Biomolecule Hybrid Systems: Synthesis, Properties and Applications. *Angew. Chem., Int. Ed.* **2004**, *43*, 6042–6108.
6. Anker, J. N.; Hall, W. P.; Lyandres, O.; Shah, N. C.; Zhao, J.; Van Duyne, R. P. Biosensing with Plasmonic Nanosensors. *Nat. Mater.* **2008**, *7*, 442–453.
7. Hu, M.; Chen, J. Y.; Li, Z. Y.; Au, L.; Hartland, G. V.; Li, X. D.; Marquez, M.; Xia, Y. N. Gold Nanostructures: Engineering their Plasmonic Properties for Biomedical Applications. *Chem. Soc. Rev.* **2006**, *35*, 1084–1094.
8. Thaxton, C. S.; Rosi, N. L.; Mirkin, C. A. Optically and Chemically Encoded Nanoparticle Materials for DNA and Protein Detection. *MRS Bull.* **2005**, *30*, 376–380.
9. Endo, T.; Ikeda, R.; Yanagida, Y.; Hatsuzawa, T. Stimuli-Responsive Hydrogel-Silver Nanoparticles Composite for Development of Localized Surface Plasmon Resonance-Based Optical Biosensor. *Anal. Chim. Acta* **2008**, *611*, 205–211.
10. Jain, P. K.; Huang, W. Y.; El-Sayed, M. A. On the Universal Scaling Behavior of the Distance Decay of Plasmon Coupling in Metal Nanoparticle Pairs: A Plasmon Ruler Equation. *Nano Lett.* **2007**, *7*, 2080–2088.
11. Elghanian, R.; Storhoff, J. J.; Mucic, R. C.; Letsinger, R. L.; Mirkin, C. A. Selective Colorimetric Detection of Polynucleotides Based on the Distance-Dependent Optical Properties of Gold Nanoparticles. *Science* **1997**, *277*, 1078–1081.
12. Connoly, S.; Fitzmaurice, D. Programmed Assembly of Gold Nanocrystals in Aqueous Solution. *Adv. Mater.* **1999**, *11*, 1202–1205.
13. Ung, T.; Liz-Marzan, L. M.; Mulvaney, P. Redox Catalysis Using Ag@SiO_2 Colloids. *J. Phys. Chem. B* **1999**, *103*, 6770–6773.
14. Lioubashevski, O.; Chegel, V. I.; Patolsky, F.; Katz, E.; Willner, I. Enzyme-Catalyzed Bio-Pumping of Electrons into Au-Nanoparticles: A Surface Plasmon Resonance and Electrochemical Study. *J. Am. Chem. Soc.* **2004**, *126*, 7133–7143.
15. Ung, T.; Giersig, M.; Dunstan, D.; Mulvaney, P. Spectroelectrochemistry of Colloidal Silver. *Langmuir* **1997**, *13*, 1773–1782.
16. Leroux, Y.; Lacroix, J. C.; Fave, C.; Trippe, G.; Felidj, N.; Aubard, J.; Hohenau, A.; Krenn, J. R. Tunable Electrochemical Switch of the Optical Properties of Metallic Nanoparticles. *ACS Nano* **2008**, *2*, 728–732.
17. Zayats, M.; Kharitonov, A. B.; Pogorelova, S. P.; Lioubashevski, O.; Katz, E.; Willner, I. Probing Photoelectrochemical Processes in Au-CdS Nanoparticle Arrays by Surface Plasmon Resonance: Application for the Detection of Acetylcholine Esterase Inhibitors. *J. Am. Chem. Soc.* **2003**, *125*, 16006–16014.
18. Baron, R.; Lioubashevski, O.; Katz, E.; Niazov, T.; Willner, I. Logic Gates and Elementary Computing by Enzymes. *J. Phys. Chem. A* **2006**, *110*, 8548–8553.
19. Strack, G.; Pita, M.; Ornatska, M.; Katz, E. Boolean Logic Gates Using Enzymes as Input Signals. *ChemBioChem* **2008**, *9*, 1260–1266.
20. Niazov, T.; Baron, R.; Katz, E.; Lioubashevski, O.; Willner, I. Concatenated Logic Gates Using Four Coupled Biocatalysts Operating in Series. *Proc. Natl. Acad. Sci. U.S.A.* **2006**, *103*, 17160–17163.
21. Strack, G.; Ornatska, M.; Pita, M.; Katz, E. Biocomputing Security System: Concatenated Enzyme-Based Logic Gates Operating as a Biomolecular Keypad Lock. *J. Am. Chem. Soc.* **2008**, *130*, 4234–4235.
22. Privman, V.; Strack, G.; Solenov, D.; Pita, M.; Katz, E. Optimization of Enzymatic Biochemical Logic for Noise Reduction and Scalability: How Many Biocomputing Gates Can be Interconnected in a Circuit. *J. Phys. Chem. B* **2008**, *112*, 11777–11784.
23. Pischel, U. Chemical Approaches to Molecular Logic Elements for Addition and Subtraction. *Angew. Chem., Int. Ed.* **2007**, *46*, 4026–4040.
24. De Silva, A. P.; Uchiyama, S.; Vance, T. P.; Wannalerse, B. A Supramolecular Chemistry Basis for Molecular Logic and Computation. *Coord. Chem. Rev.* **2007**, *251*, 1623–1632.
25. Pita, M.; Katz, E. Multiple Logic Gates Based on Electrically Wired Surface-Reconstituted Enzymes. *J. Am. Chem. Soc.* **2008**, *130*, 36–37.
26. Zhao, J.; Luo, L.; Yang, X.; Wang, E.; Dong, S. Determination of Surface pK_a of SAM Using an Electrochemical Titration Method. *Electroanalysis* **1999**, *11*, 1108–1111.
27. Pita, M.; Abad, J. M.; Vaz-Dominguez, C.; Briones, C.; Mateo-Martí, E.; Martín-Gago, J. A.; del Puerto Morales, M.; Fernández, V. M. Synthesis of Cobalt Ferrite Core/Metallic Shell Nanoparticles for the Development of a Specific PNA/DNA Biosensor. *J. Colloid Interface Sci.* **2008**, *321*, 484–492.
28. Fernández, V. M.; Martín-Gago, J. A.; Pita, M.; Serna, J. C.; Briones, C.; Vaz-Dominguez, C.; Mateo-Martí, E. Biosensor Nanoparticle, Manufacturing Proceeding and Applications. World Patent Application (200502269) and PTC Application (PTC/ES2006/070134).
29. Xia, Y.; Halas, N. J. Shape-Controlled Synthesis and Surface Plasmonic Properties of Metallic Nanostructures. *MRS Bull.* **2005**, *30*, 338–348.
30. Walczak, M. M.; Popenoe, D. D.; Deinhammer, R. S.; Lamp, B. D.; Chung, C.; Porter, M. C. Reductive Desorption of Alkanethiolate Monolayers at Gold: A Measure of Surface Coverage. *Langmuir* **1991**, *7*, 2687–2693.
31. Wagner, J.; Autenrieth, T.; Hempelmann, R. J. Core Shell Particles Consisting of Cobalt Ferrite and Silica as Model Ferrofluids [$CoFe_2O_4$-SiO_2 Core Shell Particles]. *Magn. Magn. Mater.* **2002**, *252*, 4–6.
32. Massart, R. Preparation of Aqueous Magnetic Liquids in Alkaline and Acidic Media. *IEEE Trans. Magn.* **1981**, *17*, 1247–1248.
33. Duff, D. G.; Baiker, A.; Edwards, P. P. A New Hydrosol of Gold Clusters. 1. Formation and Particle Size Variation. *Langmuir* **1993**, *9*, 2301–2309.
34. Lyon, J. L.; Fleming, D. A.; Stone, M. B; Schiffer, P.; Williams, M. E. Synthesis of Fe Oxide Core/Au Shell Nanoparticles by Iterative Hydroxylamine Seeding. *Nano Lett.* **2004**, *4*, 719–723.
35. Jimenez, J.; Sheparovych, R.; Pita, M.; Narvaez Garcia, A.; Dominguez, E.; Minko, S.; Katz, E. Magneto-Induced Self-Assembling of Conductive Nanowires for Biosensor Applications. *J. Phys. Chem. C* **2008**, *112*, 7337–7344.